Computers in Biology and Medicine 148 (2022) 105957

Contents lists available at ScienceDirect

Computers in Biology and Medicine

journal homepage: www.elsevier.com/locate/compbiomed

Identification of atrial fibrillation drivers by means of concentric ring electrodes

Gema Prats-Boluda [a,*], María S. Guillem [b], Miguel Rodrigo [c], Yiyao Ye-Lin [a], Javier Garcia-Casado [a]

[a] Centro de Investigación e Innovación en Bioingeniería, Universitat Politècnica de València, Valencia, Spain
[b] ITACA Institute, Universitat Politècnica de València, Valencia, Spain
[c] CommLab, Engineering Electronic Department, Universitat de València, Valencia, Spain

ARTICLE INFO

Keywords:
Atrial fibrillation
AF driver
Surface Laplacian potential
Concentric ring electrodes

ABSTRACT

Background and objective: The prevalence of atrial fibrillation (AF) has tripled in the last 50 years due to population aging. High-frequency (DFdriver) activated atrial regions lead the activation of the rest of the atria, disrupting the propagation wavefront. Fourier based spectral analysis of body surface potential maps have been proposed for DFdriver identification, although these approaches present serious drawbacks due to their limited spectral resolution for short AF epochs and the blurring effect of the volume conductor. Laplacian signals (BC-ECG) from bipolar concentric ring electrodes (CRE) have been shown to outperform the spatial resolution achieved with conventional unipolar recordings. Our aimed was to determine the best DFdriver estimator in endocardial electrograms and to assess the BC-ECG capacity of CRE to quantify AF activity non-invasively.
Methods: 31 AF episodes were simulated using realistic tridimensional models of the atria electrical activity and torso. Periodogram and autoregressive (AR) spectral estimators were computed and the percentile ($P90^{th}$, $P95^{th}$ and $P98^{th}$) to impose on the dominant frequencies (DFs) across whole atria to define the best DFdriver estimator evaluated. The identification of DFdriver on DFs from BC-ECG and unipolar surface signals with conventional disc electrodes was compared.
Results: The best DFdriver estimator was $P95^{th}$ and AR order 100. BC-ECG signals allowed better detection of AF activity than unipolar signals, with a significantly greater percentage of electrode locations in which DFdriver was identified (p-value 0.0095).
Conclusions: The use of BC-ECG signals for body surface Laplacian potential mapping with CRE could be helpful for better AF diagnosis, prognosis and ablation procedures than those with conventional disk electrodes.

1. Introduction

Atrial fibrillation (AF) is the most common cardiac arrhythmia and is associated with increased morbidity and mortality and a large economic burden [1] estimated to account for up to 2% of the total healthcare expenditure in European countries [2] and affecting about 46.3 million people worlwide in 2016 [3]. An aging population is a risk factor for AF, which can be explained on the one hand by the fact that structural and electrical remodeling of the atrial myocardium occurs with age: structurally aged atrial bundles increase the fibrous tissue spread between myocytes in is an age-dependent cardiomyocyte loss process [4]. On the other hand, age-related electrical changes due to ionic current alterations have been observed, including modifications in the cellular action potential shape and duration as well as a higher dispersion of cardiac repolarization [5,6]. Ederly people also present other comorbilities such as arterial stiffness, diastolic dysfunction, diabetes mellitus, coronary artery disease or valvular disease [7,8]. Moreover literature also stated that a progression of AF from paroxysmal to persistent is quicker in geriatric patients and those with underlying heart disease [9]. Therefore, an increase in the prevalence of this disease, which has already tripled in the last 50 years, can be expected [3].

The presence of high-frequency (6–12 Hz) regions driving the fibrillatory process in the rest of the atria has been observed in both animal models and human intracardiac recordings [10,11]. In these cases, rapidly activated atrial regions lead the activation of the rest of

* Corresponding author.
E-mail addresses: gprats@ci2b.upv.es (G. Prats-Boluda), mguisan@itaca.upv.es (M.S. Guillem), miguel.rodrigo@uv.es (M. Rodrigo), yiye@ci2b.upv.es (Y. Ye-Lin), jgarciac@ci2b.upv.es (J. Garcia-Casado).

https://doi.org/10.1016/j.compbiomed.2022.105957
Received 3 February 2022; Received in revised form 19 July 2022; Accepted 6 August 2022
Available online 15 August 2022

Glossary

AF	Atrial fibrillation
BC-ECG	Bipolar signals from concentric ring electrodes
CRE	Concentric ring electrodes
AR	Autoregressive spectral estimators
PD	Periodogram
DF	Dominant frequency
FEM	Finite element method
BEM	Boundary element method
EGC	Electrical activity recording of the cardiac cells recorded on the chest and the electrograms
EGM	Electrical activity on the heart surface
DFdriver	Dominant frequency of the atrial fibrillation driver
BSPM	Body surface potential maps
HDF	High dominant frequency associated to atrial fibrillation
MSE	Mean squared error
LA	Left atrium
RA	Right atrium

the atria, activated at lower frequencies due to the disruption of the propagation wavefront. These high frequency sources can be located either in the pulmonary vein area or elsewhere and their isolation by catheter ablation can terminate the arrhythmia. Identification of these high frequency sources prior to the ablation procedure would help therapy planning by allowing the prediction of the region maintaning AF that needs to be ablated [12,13].

The identification of high frequency sources in endocardial electrograms (EGM) during invasive electrophysiological procedures has been accomplished by applying Fourier Transform-based approaches [12,13]. However, Fourier based spectral analysis has the disadvanteg of poor resolution for time varying spectra computed in short analysis windows [14]. In some works autoregressive spectral analyses were used as an alternative to Fourier Transform with good spectral resolution in short electrograms segments [15] but so far no available method can identify unambigously the dominant frequency of the AF driver (DFdriver).

Non-invasive electrocardiogram (ECG) recording systems with high spatial resolution would be helpful in non-invasive AF diagnosis. To this end, body surface potential maps (BSPM) have been proposed in the literature; these consists of placing ECG signals from disc electrodes in tens or even a hundred positions on the torso. BSPM offer additional diagnostic information to that in 12-lead standard systems [16–18]. Nevertheless, the smearing effect caused by the torso volume conductor still limits the spatial resolution obtained by simply increasing the number of recording electrodes on the torso [19].

Atrial electrical activity is projected onto the torso surface and thus noticeable on the ECG, although generally masked by the ventricular content, which appears with a larger amplitude [20]. Atrial sources can thus be better observed on the ECG after cancellation of the QRST complex or when the ventricular activity is interrupted by administration of drugs, such as adenosine. In this context, we have previously shown that high frequency sources appear localized on the most proximal torso regions [21]. However, even in surface signals selected on the torso close to these sources, such activity can be masked by the activity of more distant but larger atrial regions due to poor spatial resolution in cardiac signal sensing [22,23].

In this regard, surface Laplacian, as the second spatial derivative of the surface potentials [24], could enhance the high spatial frequency components improving the spatial resolution in locating high rate sources. Laplacian electrodes can be interpreted as a filter that allocates more weight to the bioelectrical dipoles adjacent to the recording points and provide more detail in differentiating multiple concurrent dipole sources [25]. Initially, Hjorth proposed a five-point method numerical approximation technique to analyze and apply the surface Laplacian in electroencephalographic (EEG) studies, after which He and Cohen [26] developed a bipolar concentric ring electrode (CRE) to directly obtain an approximation to the body surface cardiac Laplacian potential. A CRE consists of an inner disk and at least one outer ring recording pole [27] and has the advantage over conventional unipolar electrodes that it can diminish far-field activity [28] and therefore the contribution of distant atrial sources, thus enhancing local electrical components. This reduction of the volume conductor effect may ultimately better localize the atrial electrical components reaching the torso surface and identify these high frequency components for better plannning of ablation therapies. In fact, studies in the literature have shown that CREs are able to discern between the P1 and P2 waves associated with each atrium, which usually manifest together in a single P wave in the precordial recordings [29].

The present work aims to overcome the limitations of the aforementioned previous studies: A) to determine the best spectral estimator of the DFdriver in endocardial electrograms. Our intention was to compare non parametric (periodogram, PD) and parametric (autoregressive, AR) spectral estimation techniques and identify the percentiles (90th, 95th or 98th) to be imposed on the DFs estimated across whole atria to define the highest dominant frequency, quantifying the estimation errors with respect to annotations made by experts; B) To assess the capcity of BC-ECG signals from CRE to improve the spatial resolution associated with the use of unipolar recordings by disc electrodes, enhancing the ability to non-invasively characterize atrial fibrillation activity. In this regard, we used realistic tridimensional electrophysiological models of the atria to compute electrical potentials on the torso, on which unipolar and CREs were placed during different simulated AF episodes.

2. Materials and methods

2.1. Modeling

2.1.1. Epicardial activation models

Previously validated and published 3D realistic models of the atrial anatomy composed of 284,578 nodes (673 ± 130 μm inter-node) and 1353.783 tetrahedra were used to simulate atrial electrical activity during AF episodes [24–26]. Each node was simulated as a single atrial cell using the cellular model described by Koivumaki et al. [30]. Heterogeneity in the electrophysiological properties of the atrial myocardium was introduced in the form of changes in ion currents (up to +110% IK1, -59% ICaL, +100% INa) and distribution of fibrosis (0–60% of disconnected nodes) to generate AF episodes maintained by reentrant activity with non-uniform propagation patterns and different shapes and extents of the dominant region [31]. 31 different models of AF episodes of 10 s-lengths driven by a single and spatially-stable reentrant driver in different locations were used in this work. The last 4 s of each episode was studied when AF simulation was stabilised. For each simulation, a uniform mesh of 2048 nodes (5.3 ± 3.2 mm inter-node) of unipolar electrograms (EGM) was calculated at 1 mm from the surface of the epicardium under the assumption of a homogeneous, unlimited and quasi-static conductive medium adding all effective dipole contributions over the entire model. The computed electrograms were stored for processing at a sampling frequency of 500 Hz [31] to identity AF driver sources, thus reducing the computational cost associated with higher sampling rates (above 1 kHz), used in epicardial ECG recordings or simulations and being especially advisable when analysing abnormal ventricular electrical conduction.

2.1.2. Torso modeling and surface electrocardiograms

To simulate the surface electrocardiographic activity of an AF patient we used a realistic 3D torso model on which we projected atrial activity. Our torso model was a non-homogeneous mesh to account for the higher

spatial resolution in the position of the unipolar (disc) and concentric ring electrodes (16412 nodes). The distance between vertices was 0.3421 ± 0.1283 cm (mean ± deviation) in the refined region (where surface electrodes were simulated) and 2.5857 ± 0.3522 cm elsewhere. In Fig. 1 it can be seen how denser meshing was used in the different regions where the electrodes were simulated. Fig. 1 also shows the placement of the atria in the refined torso model. The ECG potentials on the torso surface were calculated by solving the Boundary Elements Method (BEM) in the proposed torso mesh [32,33].

27 electrodes were simulated to be placed on the front, back and sides of the torso, similar to previous works with conventional disk electrodes [34], see Fig. 2.

Two types of electrode, disc and concentric, were simulated. To that commercial bipolar concentric (BC) electrodes with an outer and inner ring diameter of 42 mm and 28 mm, and a central disk diameter of 16 mm (CODE501526, Spes Medica, Italy) were considered. Simulated disc electrodes coincide with the inner pole of BC electrodes. Disc and ring BC electrodes were represented on the mesh determined by the number of nodes that belonged to each pole (see Fig. 2).

Firstly, the averaged potential of the nodes on the torso surface covered by the conductive area of each pole (disk or ring) of the electrode was determined to obtain the ECG in each electrode. To do this, nodes belonging to the different electrodes were identified from a file that contained their central location in the mesh and considering the electrode area and configuration.

Secondly, the 'conventional' ECG recordings from the disc electrodes were referenced to the Wilson Central Terminal (from now on referred to as 'unipolar recordings'), which was also simulated as the average of the potentials of the nodes in disc recordings at the right shoulder, left shoulder and the farthest point in the torso on the left side (S1, S2 and S5). The recordings with concentric electrodes were bipolar, obtaining the bipolar concentric ECG signals (BC-ECG) as the difference between the potential captured by the peripheral ring and the central disc.

2.2. Signal processing

2.2.1. Preprocessing

The pre-processing of the epicardial EGMs for the identification of the atrial depolarization rate consisted of the standard approach with a bandpass filtering between 40 Hz and 250 Hz (zero-phase, Butterworth order 8), a signal rectification and then a low-pass filtering with a cut-off frequency of 20 Hz (zero-phase, Butterworth order 8) [35]. These preprocessing steps enhance the fundamental frequency of the signal while diminishing the power of its harmonics.

Since the bandwidth requirement for dominant frequency identification in human atrial fibrillation is in the range from 3 to 13 Hz [21,36], our preprocessing of simulated surface ECG signals consisted of subtracting their mean value and subsequent 5-order high pass zero phase Butterworth filter, with a cut-off frequency of 1 Hz and 5-order low pass zero phase Butterworth filter with a cut-off frequency of 15 Hz. These cutoff frequencies were chosen considering the physiological range of the atrial activation [21]. It must be taken into account that simulated signals only contain information of atrial activity but no ventricular information (without QRS and T waves). Despite the fact that surface ECG distributes its energy between 0.05 and 150 Hz, we would like to emphasise that we did not attempt to preserve the signal morphology of the physiological P wave. Previous studies that attempted to determine the DFdriver from real-world ECG data usually set a high-pass filter with a cut-off frequency at 3 Hz, which is more restrictive than the one used in the present study.

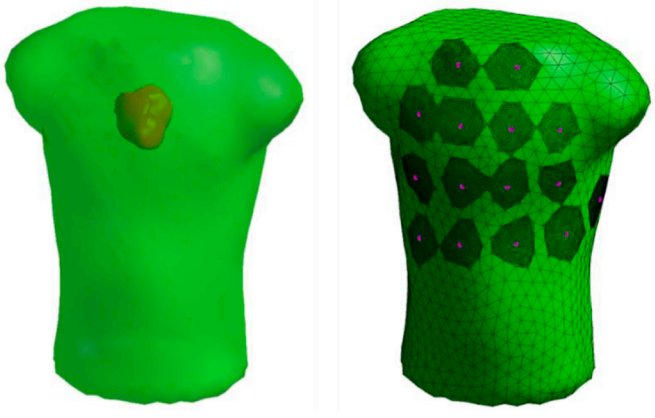

Fig. 1. Model representation of the refined torso (right) and model of the atrium (left).

2.2.2. Identification of atrial fibrillation driver frequency

In order to obtain a gold standard for the dominant frequency of the AF driver (DFdriver), firstly the transmembrane potential signal from the raw simulation was manually checked on the position of the reentrant driver for every AF model, defined by the S1–S2 pacing pattern. The number of action potentials were measured as the number of activations per second. This value was used as DFdriver to compare with that extracted from the EGMs and ECGs. To further characterize each AF model, the percentage of atrial nodes at that frequency, DFdriver ±0.25 Hz, were computed to estimate the size of the DFdriver region [31].

The performance of non-parametric (periodogram, Hamming window) and parametric (autoregressive AR model, covariance) spectral estimation methods for the identification of the driver activation frequency of the atrial activity on 4s of EGM were analysed. Parametric AR models with order N consist of predicting the actual sample by taking into account the last N samples. Too high AR orders will produce spurious peaks in the power spectral density. In general, it is strongly recommended to have one signal cycle to realiably capture its frequency. Since DFdriver usually presents a dominant frequency around 5–8 Hz, we tested AR parametric models with orders of 60, 80, 100 and 120 (equivalent to 120 ms, 160 ms, 200 ms and 240 ms with a sampling rate of 500 Hz).

Dominant frequency (DF) was obtained by considering the frequency of the maximum peak of the spectral power and possible significant peaks with power >35% of maximum peak on the AF physiological band (1–15 Hz). Subsequently it was checked whether this maximum peak corresponds to a harmonic of a lower fundamental frequency; it was considered a harmonic if it was between 1.9 and 2.1 times the frequency of a lower frequency significant peak.

The dominant frequency obtained from EGM at the 2048 atrial nodes reflects the activation frequency at different atrial sites and will include high and low frequency activities over the atria. The next step was to estimate the DFdriver from these measurements. For this, we defined (and computed) the high dominant frequency (HDF) as the frequency associated with the 90th, 95th and 98th percentiles of the DFs ($P90^{th}$, $P95^{th}$ and $P98^{th}$) in all atria nodes from periodogram and AR estimations. These percentiles may allow us to determine a robust estimator of the HDF against outliers that can be associated with the maximum value of the dominant frequency. Then Bland-Altman plots and mean squared errors were obtained to select the best estimator of the DFdriver out of the nine versions of HDF (HDF_{90_PD}, HDF_{90_AR100}, HDF_{90_AR120}, HDF_{95_PD}, …, HDF_{98_AR120}) as well as statistical differences analysed by the Wilcoxon signed rank (paired) test.

Dominant frequencies from parametric (AR model, covariance) and nonparametric (periodogram) spectral estimation methods for surface ECG signals were calculated in the same way as for EGMs. The percentage of unipolar and BC electrodes at DFdriver ±0.25Hz [31] were computed for both PD and AR spectral estimators. Subsequently a Wilcoxon signed rank (paired) test was worked out to determine whether the percentage corresponding to BC surface records was significantly higher than in simultaneous unipolar records.

Finally, it was determined whether the location of the rotor in the left

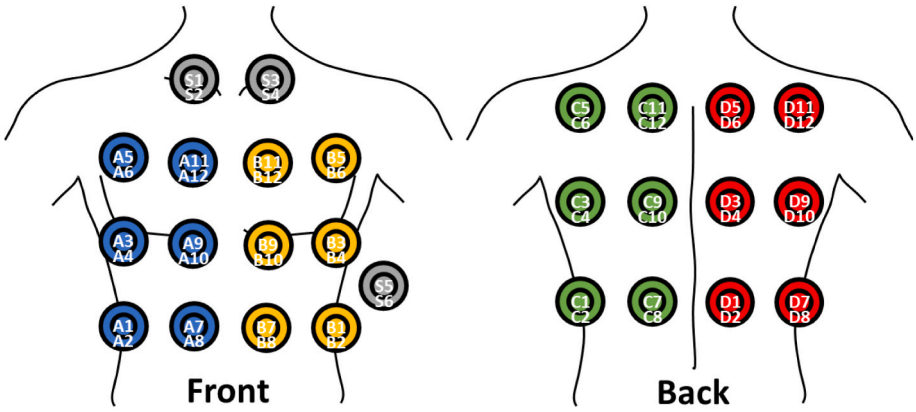

Fig. 2. Location and identification of the electrodes in the simulated torso.

(LA) or right (RA) atrium affected its identification for both unipolar and concentric bipolar surface recordings. To do so, the number of models in which at least one electrode captured the rotor frequency in the RA and LA was determined, as well as the average percentage of electrodes at the rotor frequency for both unipolar and BC-ECG signals.

3. Results

3.1. Intracardiac DFdriver estimation

Fig. 3 shows an example of the distribution of the DFs in the atrial nodes when computed with the PD and AR100 together with the DFdriver for AF model 30. It can be seen that the distribution of DF values estimated by both non-parametric and parametric methods were very similar. When we also computed DF and HDF with AR orders 60, 80 and 120 the Results were very similar but little worse than AR 100 and therefore are not reported here and there was practically no difference between dominant frequencies at the $P95^{th}$ and $P98^{th}$ percentiles. In the 90th percentile, although in most cases similar values were obtained as for the 95th and 98th percentiles, in certain models such as 15, 28, 29 and 30 (this last shown in Fig. 3), the 90th percentile of DF was not clearly related to the driver activation frequency.

To assess the best DFdriver estimation for internal EGMs between those worked out, Bland-Altman plots and the mean squared errors between DFdriver and the HDFs for each model and spectral estimator were computed (see Fig. 4). It can be seen that the frequency differences between the HDFs and the DFdrivers are greater for $P98^{th}$ than for $P95^{th}$ for both AR and PD estimations. The best results were from the $P95^{th}$ and parametric AR100 estimator, (MSE of 0.005 Hz) followed by the $P95^{th}$ from PD (MSE of 0.010 Hz), with no significant differences between them ($p < 0.001$, Wilcoxon signed test), but with significantly different results from the $P98^{th}$.

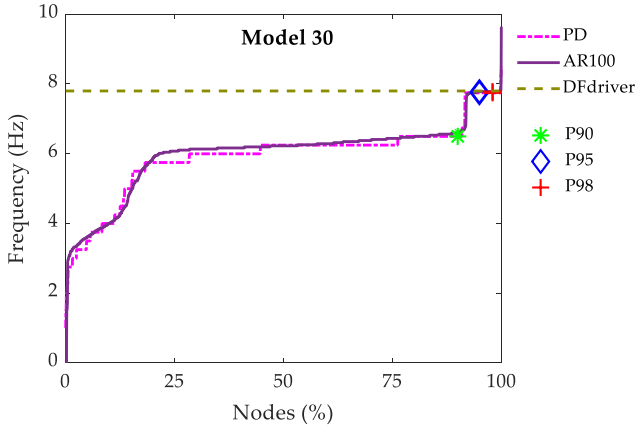

Fig. 3. Example (Model 30) of distribution of atrial nodes' dominant frequencies using periodogram (PD), and parametric AR estimation order 100 (AR100). Green stars show the 90th percentile of the internal node frequency, blue diamonds show the 95th percentile and the red cross the 98th percentile. Horizontal dashed line is the driver dominant frequency (DFdriver).

3.2. Surface DFdriver estimation

Parametric (AR 100 and 120) and non-parametric (periodogram, PD) methods were used to obtain the DF in the surface signals, as in EGMs. The results were very similar for PD and AR100 and slightly worse for AR120. In fact, using either PD or AR100 does not affect the number of models in which the DFdriver was detected in at least one electrode site. As there are no statistically significant differences (Wilcoxon Signed Rank) between the number of electrodes that capture DFdriver with both spectral estimators, either for BC-ECG or for unipolar recordings, the AR100 spectral estimator was used for surface signals as well as for the EGMs.

Fig. 5 and Fig. 6 show detailed examples of the DF distributions in the epicardium and those from the abdominal surface. Specifically, Fig. 5 depicts an example of an AF model (model 11) in which the activity of the atrial rotor is clearly picked up in several electrode positions on the surface in both BC and unipolar recordings. In this model the amount of atrial tissue with DF inside DFdriver range is quite extensive (about >28%). By contrast, Fig. 6 shows a model (model 5) in which the anomalous atrial electrical activity is quite localised (about 10% of internal nodes at DFdriver), this activity not being identified in the unipolar recordings but was identified in 15% of the BC-ECG signals. As can be seen in the right hand panels of this figure, in the unipolar recording the peak of highest frequency activity is masked by that at lower frequencies from a greater atrial area.

Fig. 7 summarizes the percentage of epicardial nodes and those of the surface unipolar and BC recording sites in which a DF, computed with AR100, was in the range of the DFdriver ± 0.25 Hz (DFdriver-range) for each of the 31 models. This figure has been arranged according to the possibility to identify DFdriver on body surface by means of BC and unipolar ECGs. In 18 out of the 31 models DFdriver could be identified (DF inside DFdriver range) from both ECG electrode configuration in at least one recording site. The percentage of sites where DFdriver was more frequently identified in BC or unipolar electrodes greatly varies for different models of this 'category'. In 7 models the DFdriver could only be identified by means of BC electrodes, while detecting DFdriver by unipolar ECG only and not by BC was found in only 1 case (model 28). Failure to identify DFdriver by both unipolar and BC ECGs occurred in 5 models. There was no apparent relationship between the size of the atrial region at DFdriver and its detectability on the body surface with the two different electrode configurations. While it was true that in all

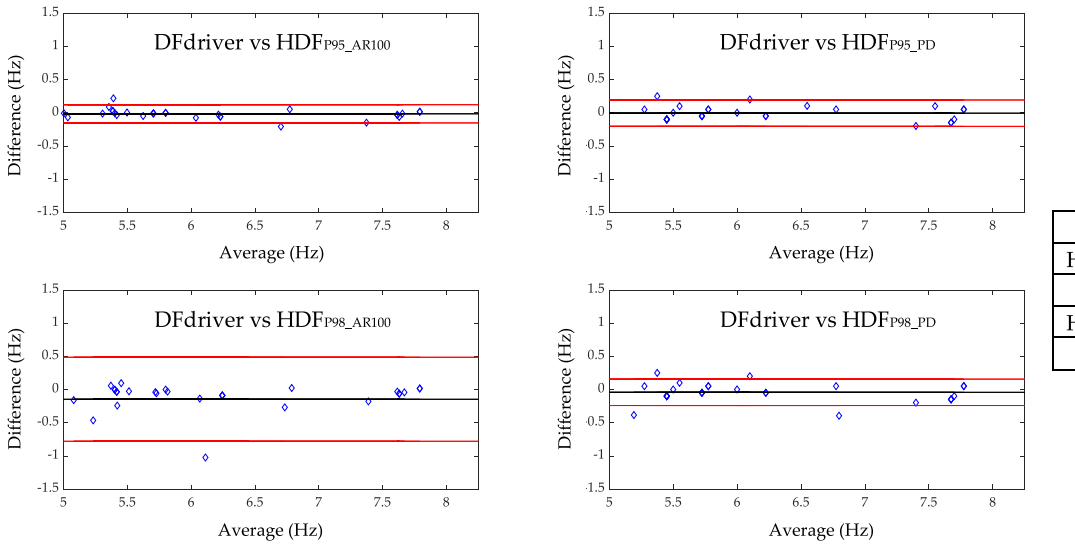

Estimator	MSE (Hz)
HDF_{P95_AR100}	0.005
HDF_{P95_PD}	0.010
HDF_{P98_AR100}	0.126
HDF_{P98_PD}	0.020

Fig. 4. Bland-Altman plots corresponding to the HDF, estimated with the 95th and 98th percentiles of the periodogram (PD) and parametric (AR 100) estimators, when compared to DFdriver, and table with HDFs root mean squared errors (MSE) with respect to DFdriver.

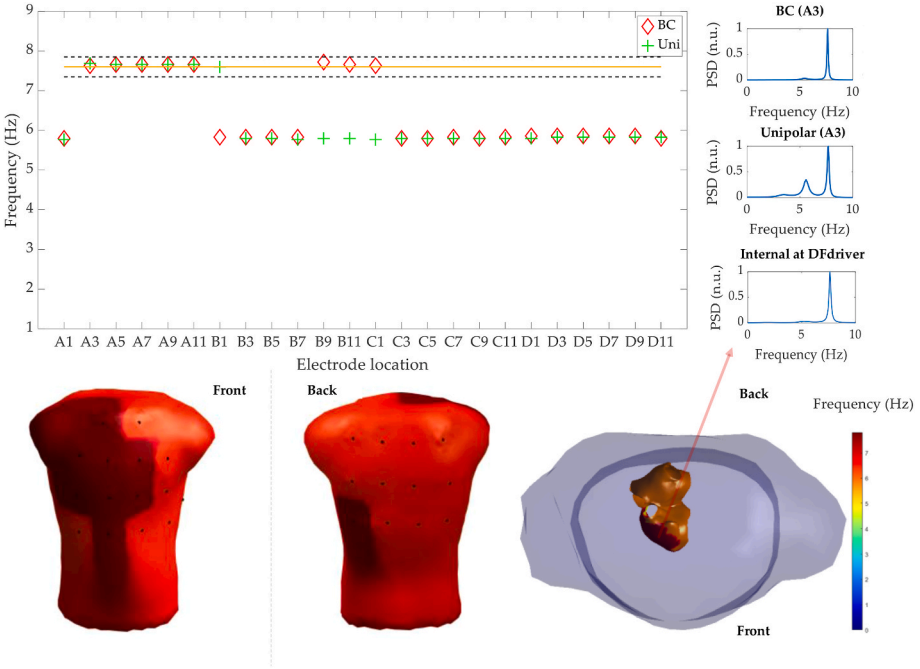

Fig. 5. Lower panels: colour maps of DF (AR100) on the torso (BC-ECG signals) and on the atrium for Model 11. Right panels: power spectrum of signals at: one atrial (internal) node with DF inside DFdriver range, electrode location A3 (unipolar and BC-ECG). Top central panel: DF values of unipolar (crosses) and BC (diamonds) surface signals from electrode locations. Orange line shows the frequency of the DFdriver and the broken lines the margins of DFdriver-range (DFdriver ± 0.25 Hz).

models with more than 30% of atrial nodes in DFdriver range, the frequency of the driver was detected by both configurations, in models with <30% of nodes it could be detected by both, only by BC or by none of the electrode configurations. For models with abnormally small atrial regions (5–10%), activity at DFdriver was detected on the body surface by both, only one or no electrode configuration, which indicates the important role of the position of the driving region. However, it should be highlighted that the BC configuration succeeded in identifying DFdriver in 25 of the 31 models (80%), while unipolar only did so in 19 (61%). Indeed, the Wilcoxon signed rank (paired) test indicated that the percentage of electrodes in which the DFdriver was identified in BC surface records was significantly higher than in simultaneous unipolar records (p-value 0.0095).

We further investigated the influence of the location of the AF driver in the left (14 models, LA) or right atrium (17 models, RA) in identifying its frequency in unipolar and BC-ECG recordings. The results are summarised in Table 1. When rotor activity was in the LA, surface rotor activity (DF at DFdriver ± 0.25 Hz) was identified in at least one torso position in 57% of the cases for unipolar electrodes and in 71% of those for BC electrodes, the average percentage of electrodes at the DFdriver being ± 0.25 Hz of 6.7% and 11.0% for unipolar and BC electrodes, respectively. For models with rotor activity in the right atrium (RA), surface rotor activity was identified in at least one torso position in 65% of the cases for unipolar electrodes and in 88% for BC, with an average percentage of electrodes at DFdriver of ±0.25 Hz of 17.9% and 25.6% for unipolar and BC electrodes. As expected therefore, BC electrodes

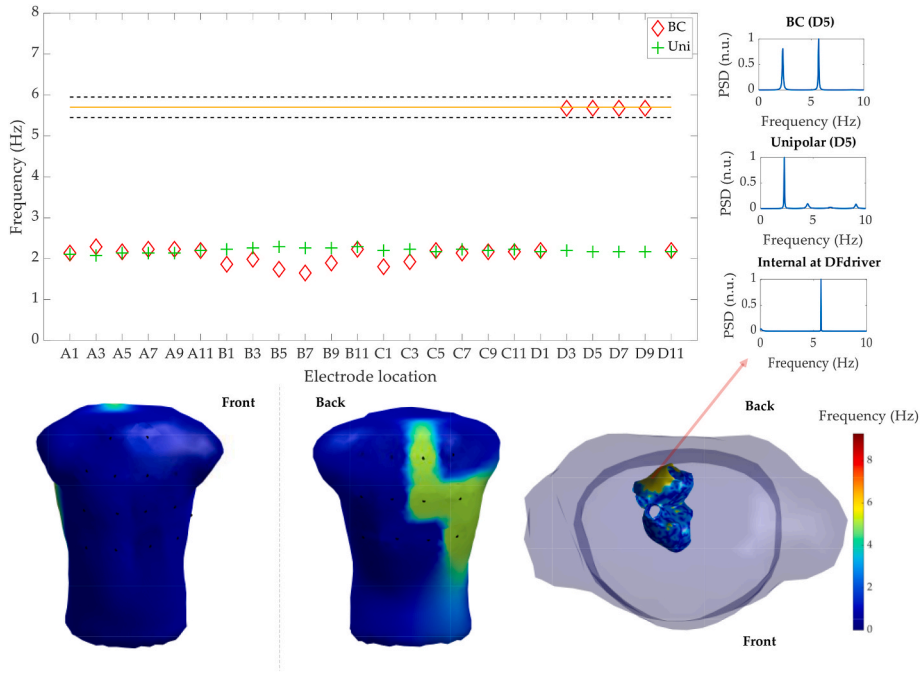

Fig. 6. Lower panels: color maps of DF (AR100) on the torso (BC signals) and on the atrium for Model 5. Right panels: power spectrum of signals at: one atrial node (internal) with DF inside DFdriver range, electrode location D5 (unipolar and BC). Top central panel: DF values of unipolar (crosses) and BC (diamonds) surface signals from electrode locations. Orange line corresponds to the frequency of the DFdriver and the dashed lines the margins of DFdriver-range (DFdriver ± 0.25 Hz).

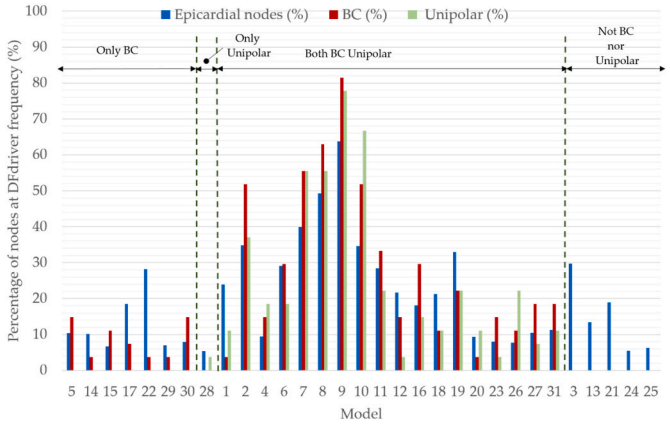

Fig. 7. of epicardial nodes and surface ECG recording sites (BC: bipolar concentric, Unipolar: disc) at atrial fibrillation driver frequency per model.

Table 1
DFdriver identification according to the atrial side. LA: left atrium; RA: right atrium.

	% of Models		% of Electrodes (mean)	
	LA	RA	LA	RA
Unipolar	57%	65%	6.7%	17.9%
BC	71%	88%	11.0%	25.6%

presented significantly higher detectability of surface rotor activity than unipolar electrodes, regardless of whether the rotor was in LA or RA. The detectable percentage of atrial high-frequency activity is lower in those with the rotor in LA than those in RA, both for unipolar and BC recordings.

4. Discussion

The important features of AF drivers present on surface electrical recordings can be used to stratify and guide ablation procedures [32]. Spectral analysis provides information on the activation rate of the atria; areas with high frequency are suspected of driving the cardiac rhythm in patients with AF and these therefore are targets for catheter ablation [15]. This manuscript compares different estimators to identify these high frequency regions in the atria from EGM recordings. It also presents a new BSPM system using concentric ring electrodes, which enhanced the accuracy of DFdriver identification on the torso signals.

4.1. DFdriver identification in EGM

Fourier Transform-based estimations have been used to identify DFdriver in endocardial electrograms during invasive electrophysiological procedures [37]. To avoid the poor resolution of time varying spectra computed in short analysis windows, autoregressive spectral analysis was proposed to estimate DF in short EGM segments [14,15]. In Salinet et al., AR and PD techniques were applied to EGM segments about 7s long, obtaining similar results for both techniques in DFdriver identification [15], which agrees with the present results [15]. However, although several techniques have been proposed for AF source identification as the highest dominant frequency, organisation and regularization indexes, phase singularities or fractionated atrial electrograms, none of these has become a gold standard, resulting in controversial results across different clinical studies [38,39]. In the present work, we analysed not only the effect of the spectral estimator, but also the performance of harmonics removal and the use of the $P90^{th}$, $P95^{th}$ and $P98^{th}$ percentiles of the DF distribution in the atrium to obtain a more robust spectral estimator of the high frequency atria activity, DFdriver (HDF), against possible outliers associated with the maximum dominant frequency. This approach is novel in the literature and the results indicate that the best DFdriver estimation was obtained with the AR method and the 95th percentile, $HDF_{95\_AR100,}$ with no significant differences with HDF_{95_PD}. ($p < 0.001$, Wilcoxon signed test), but with considerable differences regarding the use of the $P90^{th}$ and $P98^{th}$

percentiles.

4.2. AF surface mapping

As for surface ECG recordings, in the arrhythmologic field body surface potential mapping (BSPM) has been devoted to detecting signs of susceptibility to arrhythmias and identifying their sites of origin [40], for which activation maps identifying fiducial ECG points from BSPM recordings from unipolar electrodes were traditionally obtained [41]. However, several studies have shown that in the case of AF, dominant frequency analysis is more stable than activation times in describing the AF electrical activity [31]. Moreover, DF maps obtained by FFT from the BSPM of unipolar electrodes identified the atrium harbouring the DFdriver site and the presence of a gradient in activation frequencies across the atria, not only the global activation rate of the whole atrial tissue [21]. They can also assess the effectiveness of ablation therapy in restoring sinus rhythm [21,42].

Detecting the site(s) driving AF by BSPM could result in a rapid, noninvasive and personalized diagnosis and treatment of AF patients. However, surface frequency maps only provide an overall estimation of the location of the highest atrial DF site, but not those at the specific DFdriver location [21]. As previously mentioned, increasing spatial resolution to enhance detection of the arrhythmia origin not only depends on increasing the number of electrodes on the torso surface, as unipolar ECG recordings are highly affected by the blurring effect of the torso volume conductor [29,43]. Electrocardiographic Imaging (ECGI) for mathematically reconstructing epicardial activity has been shown to be an effective tool for mapping DF during AF and has been validated against intracardiac panoramic electrograms [36]. Although this technique can increase DF mapping resolution at the expense of introducing a patient-specific anatomy, robust spectral and DF estimation methods are also required for the ECGI pipeline and further research should be conducted to study whether CREs can also help in ECGI solutions and the best spectral estimators for this non-invasive technique.

4.3. Laplacian ECG recordings

Surface Laplacian ECG recordings have emerged as an alternative that can overcome the limitations of BSPM spatial resolution [44]. Body surface Laplacian mapping estimated by the spline technique reveals high-resolution surface mapping of normal atrial depolarization compared to the smooth patterns of the BSPMs, which may possibly be associated with atrial activation wavefronts [19]. Instead of using discretization techniques and monopolar electrodes, surface Laplacian can be directly estimated by concentric ring electrodes [45,46]. This type of electrode has been used to estimate the Laplacian of the surface bioelectric potential in many applications such as electroencephalography [47,48], skeletal electromyography [49] and gastroenterology [50,51].Several studies have assessed the capability of CRE electrodes to pick up high-local resolution ECG signals for electrocardiography. In this regard, local cardiac activity, as in the case of the P1 and P2 atrial waves, was identified in BC-ECG surface records, while they were difficult to distinguish in precordial leads, commonly used in out-patient clinics, since disc electrode recordings are more affected by the volume conductor effect, as previously mentioned [29,43]. In addition, BC-ECG signals recorded in a position comparable to the V1 precordial lead proved to be better at picking up atrial activity than standard 12-Lead ECG, providing the best combination of detectability and normalized amplitude of the P wave [27].

Considering the enhanced spatial sensitivity of CRE, body surface Laplacian potential maps have been used to obtain moment of activation (MOA) isochronal maps in healthy subjects, suggesting their potential use by clinicians in diagnosing arrhythmias and assessing the efficacy of therapies [52]. However, as far as we are concerned, this is the first study to assess the capacity of BC-ECG signals to identify the DFdriver in AF. In this regard, in the present work we found that in general the higher the percentage of internal nodes at the DFdriver, the higher the number of surface recordings in which DF in the DFdriver range were identified, but not always. The study of the atrial zones in the DFdriver for the 31 models analysed revealed that the capacity to identify these drivers depends on the proximity of the affected atrial area to the chest surface. For instance, in model 3 the percentage of internal electrodes at DFdriver is quite high (about 13%) but no surface electrode was able to detect this activity, which involves a deep atrial area facing into the chest cavity. Something similar occurs in models 21 and 22, which highlight that both proximity to the body surface and the orientation of the atrial tissue may influence the detection of AF foci. However, the results showed that BC-ECG recordings were better than unipolar recordings in identifying the DFdriver in AF situations (80% of the cases vs. 61%, respectively). This is probably due to enhanced spatial resolution and greater attenuation of far field CRE components, in comparison to disc electrodes. In this latter, the activity of the atrial region harbouring a DFdriver can be more easily masked by other more distant but larger atrial regions. This result agrees with theoretical studies of the two-dimensional spatial transfer function and supports CREs being more sensitive to vertical dipole sources closer to the electrode and less to distant dipoles than recordings with disk electrodes [53]. In the present work we also found that surface uptake of DFdriver-associated activities easier for the models in which the rotor is in the right atrium than those in which it is in the left. This could be attributed to the better reflection of right atrial activity on the torso, since the right atrium is closer to the anterior torso than the left atrium to the posterior torso.

4.4. Limitations and future studies

Dynamic torso models can simulate breathing in aspects such as (1) conduction conditions and (2) geometrical distances of the moving heart and moving torso surface. In this study we used a static torso model in which the effect of respiration and the variation in distance between heart and recording electrodes was not taken into account. Even though it would be advisable to consider these effects in future work, we did not think it necessary for the objectives of the present study, since it would not have had a great effect on the comparison between the different HDF estimation methods assessed, or the comparison of the capacity of unipolar and BC-ECG recordings to non-invasively pick up HDF activity. In the specific case of breathing, as its frequency is below 0.3 Hz, it does not significantly affect the proposed analysis.

BC-ECG captures the bioelectric activity focused on the central recording point of the CRE and reduces the volume conductor effect more than conventional unipolar electrodes and seems to precisely locate the sources attributable to the DFdriver of atrial fibrillation and thus the ablation target area by non-invasive recording (inverse problem). Even using realistic multi-layer BEM models or FEM models that consider the individualized anatomy of the patient's torso obtained from images, differences in terms of the arrangement and features of the different layers of tissue now provide different volume conductor effects [23,54] and solving the inverse problem from conventional ECG recordings remains a challenge for the scientific-technical community, so that invasive methods are still necessary to determine the injured area origin of the DFdriver of atrial fibrillation. Experimental recordings will confirm the present results by simulations, analysing their robustness to factors such as the blurring effect of the volume conductor or the signal-to-noise ratio of the recordings. However, there is still further to go before we can determine whether the combination of body surface Laplacian ECG mapping with CRE and cardiac images will provide a non-invasive tool for diagnosis, prognosis and ablation targeting of cardiac arrhythmias [55].

5. Conclusions

Parametric and non-parametric techniques were assessed for epicardial DFdriver identification, obtaining very similar results when

using the P95 of the DFs worked out using a periodogram and an order 100 autoregressive parametric model (AR100), this last being the one with the best coincidence with the DFdriver (MSE 0.005Hz) but without a significant difference. We assessed the capacity to identify the DFdriver non-invasively by means of BSPM with unipolar and CREs. In general, the higher the epicardial nodes at the DFdriver, the higher the number of surface recordings in which the DFdriver is detected. However, the orientation of the atrial region in which the DFdriver is located seems to be another important factor that influences the identification of this activity on surface recordings, especially when the affected atrial area is small. In any case, the results revealed that BC-ECG signals from CRE can detect atrial fibrillation activity on the surface better than unipolar signals from disc electrodes in the same positions: the BC configuration succeeded in identifying the DFdriver in 25 out of the 31 models (80%), while unipolar only did so in 19 (61%). BC-ECG signals from BSPM with CRE could therefore be helpful for better AF diagnosis, prognosis and in planning ablation procedures.

Summary

The prevalence of atrial fibrillation (AF) has tripled in the last 50 years due to population aging and survival with chronic diseases turning into an epidemic. High-frequency activated atrial regions (DFdriver) lead the activation of the rest of the atria, disrupting of the propagation wavefront. The identification of DFdriver sources would help diagnose AF and plan ablation procedures. Fourier based spectral analysis of body surface potential maps (BSPM) has been proposed for non-invasively dealing with DFdriver identification. However, these approaches present serious drawbacks due to the limited temporal resolution of the *Fourier Transform* for short AF epochs and the blurring effect of the volume conductor associated with unipolar ECG recordings in BSPM. In this work we aimed: to determine the best estimator of the DFdriver frequency in endocardial electrograms by the non-parametric (periodogram, PD) and parametric (autoregressive, AR) spectral estimators to determine the percentiles (P90th, P95th or P98th) to be imposed on the DFs estimated across the whole atria to define the highest dominant frequency (HDF); and -to assess the capability of surface unipolar and bipolar concentric ECG signals (BC-ECG) from concentric ring electrodes (CRE) to identify atrial fibrillation activity. Realistic tridimensional models of the atria electrical activity and the torso, on which unipolar and CRE were placed, were simulated during different AF episodes. The results revealed that the best DFdriver estimator (HDF) was better represented by $P95^{th}$ and parametric AR order 100 estimator, (HDF_{95_AR100}, MSE 0.005 Hz), followed by percentile $P95^{th}$ from PD (HDF_{95_PD}, MSE 0.010 Hz). The greater the epicardial area at DFdriver, the higher the number of surface recordings in which the DFdriver is detected. However, the location and orientation of the atrial fibrillation region influence its identification on the torso surface. Nevertheless, BC-ECG signals allowed better detection than unipolar signals, and the percentage of electrode locations for BC-ECG records in which DFdriver was identified was significantly higher than in simultaneous unipolar records (p-value 0.0095, Wilcoxon paired test). The use of BC-ECG signals for body surface Laplacian potential mapping with CRE could thus be helpful for better AF diagnosis, prognosis and in ablation procedures than those with conventional disc electrodes.

Funding

This work was supported by the Spanish Ministry of Economy and Competitiveness (PID2020-114291RB-I00) and the Instituto de Salud Carlos III, the European Regional Development Fund (MCIU/AEI/FEDER, UE RTI2018-094449-A-I00-AR, PI17/01106), EIT Health (Activity code 19600, EIT Health is supported by EIT, a body of the European Union) and the Generalitat Valenciana (AICO/2021/318, AICO/2021/126 and AICO/2019/220).

Declaration of competing interest

M.S.G and M.R. are shareholders of CORIFY CARE SL. The rest of the authors declare no conflict of interest and that the funders had no role in the design of the study; in the collection, analyses, or interpretation of data; in the writing of the manuscript, or in the decision to publish the results".

References

[1] G. Hindricks, T. Potpara, N. Dagres, E. Arbelo, J.J. Bax, C. Blomström-Lundqvist, G. Boriani, M. Castella, G.A. Dan, P.E. Dilaveris, L. Fauchier, G. Filippatos, J. M. Kalman, M. La Meir, D.A. Lane, J.P. Lebeau, M. Lettino, G.Y.H. Lip, F.J. Pinto, G. N. Thomas, M. Valgimigli, I.C. Van Gelder, B.P. Van Putte, C.L. Watkins, ESC Scientific Document Group. 2020 ESC Guidelines for the diagnosis and management of atrial fibrillation developed in collaboration with the European Association for Cardio-Thoracic Surgery (EACTS): The Task Force for the diagnosis and management of atrial fibrillation of the European Society of Cardiology (ESC) Developed with the special contribution of the European Heart Rhythm Association (EHRA) of the ESC, Eur Heart J 42 (5) (2021 Feb 1) 373–498, https://doi.org/10.1093/eurheartj/ehaa612. PMID: 32860505.

[2] M. Velleca, G. Costa, L. Goldstein, M. Bishara, L. Ming Boo, A review of the burden of atrial fibrillation: understanding the impact of the new millennium epidemic across europe, EMJ Eur. Med. J. 110 (2019).

[3] J. Kornej, et al., Epidemiology of atrial fibrillation in the 21st century, Circ. Res. 127 (Jun. 2020) 4–20.

[4] M.S. Spach, J.F. Heidlage, P.C. Dolber, R.C. Barr, Mechanism of origin of conduction disturbances in aging human atrial bundles: experimental and model study, Heart Rhythm 4 (2) (Feb. 2007) 175–185.

[5] C. Pearman, A. Trafford, D. Eisner, K. Dibb, 218 action potential alternans in the ageing ovine atria, Heart 100 (Suppl 3) (Jun. 2014) A119–A120.

[6] S.V. Pandit, J. Jalife, Aging and atrial fibrillation research: where we are and where we should go, Heart Rhythm 4 (2) (Feb. 2007) 186–187.

[7] A.A. Mashat, et al., Atrial fibrillation: risk factors and comorbidities in a tertiary center in Jeddah, Saudi Arabia, Int. J. Gen. Med. 12 (2019) 71.

[8] S. Fumagalli, et al., Atrial fibrillation after electrical cardioversion in elderly patients: a role for arterial stiffness? Results from a preliminary study, Aging Clin. Exp. Res. 28 (6) (Dec. 2016) 1273–1277.

[9] H. Ogawa, et al., Progression from paroxysmal to sustained atrial fibrillation is associated with increased adverse events, Stroke 49 (10) (2018) 2301–2308.

[10] R. Mandapati, A. Skanes, J. Chen, O. Berenfeld, J. Jalife, Stable microreentrant sources as a mechanism of atrial fibrillation in the isolated sheep heart, Circulation 101 (2) (Jan. 2000) 194–199.

[11] M. Mansour, R. Mandapati, O. Berenfeld, J. Chen, F.H. Samie, J. Jalife, Left-to-Right gradient of atrial frequencies during acute atrial fibrillation in the isolated sheep heart, Circulation 103 (21) (May 2001) 2631–2636.

[12] P. Sanders, et al., Electrophysiologic and clinical consequences of linear catheter ablation to transect the anterior left atrium in patients with atrial fibrillation, Heart Rhythm 1 (2) (Jul. 2004) 176–184.

[13] F. Atienza, et al., Real-time dominant frequency mapping and ablation of dominant frequency sites in atrial fibrillation with left-to-right frequency gradients predicts long-term maintenance of sinus rhythm, Heart Rhythm 6 (1) (Jan. 2009) 33–40.

[14] S.M. Kay, Modern Spectral Estimation : Theory and Application, Prentice Hall, 1987.

[15] J.L. Salinet, N. Masca, P.J. Stafford, G.A. Ng, F.S. Schlindwein, Three-dimensional dominant frequency mapping using autoregressive spectral analysis of atrial electrograms of patients in persistent atrial fibrillation, Biomed. Eng. Online 15 (1) (2016).

[16] M. Fereniec, G. Stix, M. Kania, T. Mroczka, R. Maniewski, An analysis of the U-wave and its relation to the T-wave in body surface potential maps for healthy subjects and MI patients, Ann. Noninvasive Electrocardiol. 19 (2) (Mar. 2014) 145–156.

[17] M. Meo, et al., Insights into the spatiotemporal patterns of complexity of ventricular fibrillation by multilead analysis of body surface potential maps, Front. Physiol. 11 (Sep. 2020) 1116.

[18] V. Kommata, M. Elshafie, E. Sciaraffia, M. Perez, R. Augustine, C. Blomström-Lundqvist, QRS dispersion detected in ARVC patients and healthy gene carriers using 252-leads body surface mapping: an explorative study of a potential diagnostic tool for arrhythmogenic right ventricular cardiomyopathy, PACE - Pacing Clin. Electrophysiol. 44 (8) (Aug. 2021) 1355–1364.

[19] J. Lian, et al., Body surface Laplacian mapping of atrial depolarization in healthy human subjects, Med. Biol. Eng. Comput. 40 (6) (Nov. 2002) 650–659.

[20] A. Bollmann, N.K. Kanuru, K.K. McTeague, P.F. Walter, D.B. DeLurgio, J. J. Langberg, Frequency analysis of human atrial fibrillation using the surface electrocardiogram and its response to ibutilide, Am. J. Cardiol. 81 (12) (Jun. 1998) 1439–1445.

[21] G. Ms, et al., Noninvasive localization of maximal frequency sites of atrial fibrillation by body surface potential mapping, Circ. Arrhythm. Electrophysiol. 6 (2) (Apr. 2013) 294–301.

[22] J. Liu, et al., Intrinsically stretchable electrode array enabled in vivo electrophysiological mapping of atrial fibrillation at cellular resolution, Proc. Natl. Acad. Sci. USA 117 (26) (Jun. 2020) 14769–14778.

[23] F.J. Vanheusden, et al., Systematic differences of non-invasive dominant frequency estimation compared to invasive dominant frequency estimation in atrial fibrillation, Comput. Biol. Med. 104 (Jan. 2019) 299.
[24] H. B, Brain electric source imaging: scalp Laplacian mapping and cortical imaging, Crit. Rev. Biomed. Eng. 27 (3–5) (Jan. 1999) 149–188.
[25] B. He, X. Yu, D. Wu, N. Mehdi, Body surface Laplacian mapping of bioelectrical activity, Methods Inf. Med. 36 (4–5) (1997) 326–328.
[26] H. B, C. Rj, B. He, R.J.J. Cohen, Body surface Laplacian ECG mapping, IEEE Trans. Biomed. Eng. 39 (11) (Nov. 1992) 1179–1191.
[27] G. Prats-Boluda, Y. Ye-Lin, J.M. Bueno-Barrachina, R. Rodriguez De Sanabria, J. Garcia-Casado, Towards the clinical use of concentric electrodes in ECG recordings: influence of ring dimensions and electrode position, Meas. Sci. Technol. 27 (2) (2016).
[28] D. Farina, C. Cescon, Concentric-ring electrode systems for noninvasive detection of single motor unit activity, IEEE Trans. Biomed. Eng. 48 (11) (Nov. 2001) 1326–1334.
[29] G. Prats-Boluda, Y. Ye-Lin, F. Pradas-Novella, E. Garcia-Breijo, J. Garcia-Casado, Textile concentric ring electrodes: influence of position and electrode size on cardiac activity monitoring, J. Sens. 2018 (Jul. 2018) 1–9.
[30] J.T. Koivumäki, G. Seemann, M.M. Maleckar, P. Tavi, "In silico screening of the key cellular remodeling targets in chronic atrial fibrillation, PLoS Comput. Biol. 10 (5) (2014), e1003620.
[31] M. Rodrigo, et al., Highest dominant frequency and rotor positions are robust markers of driver location during noninvasive mapping of atrial fibrillation: a computational study, Heart Rhythm 14 (8) (Aug. 2017) 1224–1233.
[32] J. Pedrón-Torrecilla, et al., Noninvasive estimation of epicardial dominant high-frequency regions during atrial fibrillation, J. Cardiovasc. Electrophysiol. 27 (4) (Apr. 2016) 435–442.
[33] B.M. Horáček, J.C. Clements, The inverse problem of electrocardiography: a solution in terms of single- end double-layer sources on the epicardial surface, Math. Biosci. 144 (2) (Sep. 1997) 119–154.
[34] M. Rodrigo, et al., Minimal configuration of body surface potential mapping for discrimination of left versus right dominant frequencies during atrial fibrillation, Pacing Clin. Electrophysiol. 40 (8) (Aug. 2017) 940–946.
[35] F. Castells, R. Cervigón, J. Millet, On the preprocessing of atrial electrograms in atrial fibrillation: understanding botteron's approach, Pacing Clin. Electrophysiol. 37 (2) (Feb. 2014) 133–143.
[36] M. Rodrigo, et al., Non-invasive spatial mapping of frequencies in atrial fibrillation: correlation with contact mapping, Front. Physiol. (Jan. 2021) 1727.
[37] X. Li, et al., Automatic extraction of recurrent patterns of high dominant frequency mapping during human persistent atrial fibrillation, Front. Physiol. 12 (Mar. 2021) 286.
[38] J.L. Salinet, J.H. Tuan, A.J. Sandilands, P.J. Stafford, F.S. Schlindwein, G. André Ng, Distinctive patterns of dominant frequency trajectory behavior in drug-refractory persistent atrial fibrillation: preliminary characterization of spatiotemporal instability, J. Cardiovasc. Electrophysiol. 25 (4) (2014) 371–379.
[39] T.P. Almeida, et al., Minimizing discordances in automated classification of fractionated electrograms in human persistent atrial fibrillation, Med. Biol. Eng. Comput. 54 (11) (Nov. 2016) 1695–1706.
[40] L. De Ambroggi, C. Santambrogio, Clinical use of body surface potential mapping in cardiac arrhythmias, Physiol. Res. 42 (1993) 137–140.
[41] R.M. Gage, A.E. Curtin, K.V. Burns, S. Ghosh, J.M. Gillberg, A.J. Bank, Changes in electrical dyssynchrony by body surface mapping predict left ventricular remodeling in patients with cardiac resynchronization therapy, Heart Rhythm 14 (3) (Mar. 2017) 392–399.
[42] S. P, et al., Spectral analysis identifies sites of high-frequency activity maintaining atrial fibrillation in humans, Circulation 112 (6) (Aug. 2005) 789–797.
[43] J.V.J. Lidón-Roger, et al., Textile concentric ring electrodes for ECG recording based on screen-printing technology, Sensors 18 (1) (Jan. 2018) 300.
[44] K. Umetani, Y. Okamoto, S. Mashima, K. Ono, H. Hosaka, B. He, Body surface laplacian mapping in patients with left or right ventricular bundle branch block, Pacing Clin. Electrophysiol. 21 (11) (Nov. 1998) 2043–2054.
[45] O. Makeyev, W.G. Besio, O. Makeyev, W.G. Besio, Improving the accuracy of laplacian estimation with novel variable inter-ring distances concentric ring electrodes, Sensors 16 (6) (Jun. 2016) 858.
[46] J. Garcia-Casado, Y. Ye-Lin, G. Prats-Boluda, O. Makeyev, Evaluation of bipolar, tripolar, and quadripolar laplacian estimates of electrocardiogram via concentric ring electrodes, Sensors 19 (17) (Sep. 2019).
[47] W.G. Besio, et al., High-frequency oscillations recorded on the scalp of patients with epilepsy using tripolar concentric ring electrodes, IEEE J. Transl. Eng. Heal. Med. 2 (2014).
[48] Y. Boudria, A. Feltane, W. Besio, Significant improvement in one-dimensional cursor control using Laplacian electroencephalography over electroencephalography, J. Neural. Eng. 11 (3) (Jun. 2014), 035014.
[49] T. Hiyama, S. Sakurazawa, M. Toda, J. Akita, K. Kondo, Y. Nakamura, Motion estimation of five fingers using small concentric ring electrodes for measuring surface electromyography, in: 2014 IEEE 3rd Global Conference on Consumer Electronics, GCCE 2014, 2014, pp. 376–380.
[50] J. Garcia-Casado, V. Zena-Gimenez, G. Prats-Boluda, Y. Ye-Lin, Enhancement of non-invasive recording of electroenterogram by means of a flexible array of concentric ring electrodes, Ann. Biomed. Eng. 42 (3) (2014).
[51] G. Prats-Boluda, J. Garcia-Casado, J.L. Martinez-de-Juan, Y. Ye-Lin, Active concentric ring electrode for non-invasive detection of intestinal myoelectric signals, Med. Eng. Phys. 33 (4) (May 2011) 446–455.
[52] W. Besio, T. Chen, Tripolar Laplacian electrocardiogram and moment of activation isochronal mapping, Physiol. Meas. 28 (5) (May 2007) 515–529.
[53] C.C. Lu, P.P. Tarjan, Pasteless, active, concentric ring sensors for directly obtained laplacian cardiac electrograms, J. Med. Biol. Eng. 22 (2002) 199–203.
[54] Z. Zhou, Q. Jin, L.Y. Chen, L. Yu, L. Wu, B. He, Noninvasive imaging of high-frequency drivers and reconstruction of global dominant frequency maps in patients with paroxysmal and persistent atrial fibrillation, IEEE Trans. Biomed. Eng. 63 (6) (Jun. 2016) 1333–1340.
[55] H. Cochet, et al., Cardiac Arrythmias: Multimodal Assessment Integrating Body Surface ECG Mapping into Cardiac Imaging, Radiology 271 (1) (Dec. 2013) 239–247, https://doi.org/10.1148/radiol.13131331.